ACS APPLIED MATERIALS & INTERFACES

Research Article

www.acsami.org

HNO_3-Assisted Polyol Synthesis of Ultralarge Single-Crystalline Ag Microplates and Their Far Propagation Length of Surface Plasmon Polariton

Cheng-Wei Chang,[†] Fan-Cheng Lin,[‡] Chun-Ya Chiu,[‡] Chung-Yi Su,[†] Jer-Shing Huang,[‡] Tsong-Pyng Perng,[†] and Ta-Jen Yen*[,†]

[†]Department of Materials Science and Engineering, National Tsing Hua University, 101, Section 2, Kuang Fu Road, Hsinchu 30013, Taiwan

[‡]Department of Chemistry, National Tsing Hua University, 101, Section 2, Kuang Fu Road, Hsinchu 30013, Taiwan

Supporting Information

ABSTRACT: We developed a HNO_3-assisted polyol reduction method to synthesize ultralarge single-crystalline Ag microplates routinely. The edge length of the synthesized Ag microplates reaches 50 μm, and their top facets are (111). The mechanism for dramatically enlarging single-crystalline Ag structure stems from a series of competitive anisotropic growths, primarily governed by carefully tuning the adsorption of Ag^0 by ethylene glycol and the desorption of Ag^0 by a cyanide ion on Ag(100). Finally, we measured the propagation length of surface plasmon polaritons along the air/Ag interface under 534 nm laser excitation. Our single-crystalline Ag microplate exhibited a propagation length (11.22 μm) considerably greater than that of the conventional E-gun deposited Ag thin film (5.27 μm).

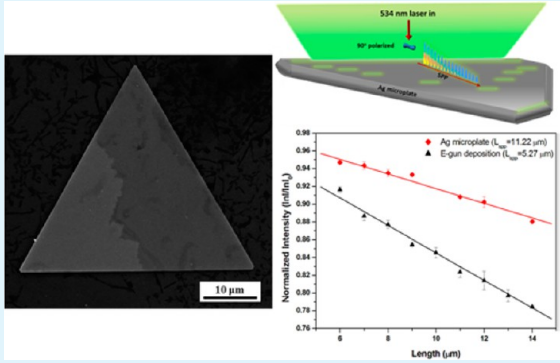

KEYWORDS: *Ag microplates, HNO_3, propagation length, single crystalline, ultralarge*

INTRODUCTION

Morphology control of metal structures in nano and micro scales is an essential factor to intensify their plasmonic responses, such as surface enhanced Raman scattering (SERS),[1] molecular photoacoustic bioimaging,[2] enzyme-free H_2O_2 sensing,[3] plasmonic nanopixels,[4] nanoantennas,[5] and even logic nanocircuitry.[6] In particular for the applications in near-infrared and visible regions, Ag structures appear to be an outstanding plasmonic material because of their low internal loss[7] and low plasma frequency.[8] To fabricate a variety of Ag structures, recently there was reported a kind of economic chemical method, facile synthesis,[9−11] in which the growth direction and the shape of Ag nanocubes, nanowires, and nanoplates can be manipulated by an aging process,[12] by $CuCl_2$-assisted heterogeneous nucleation,[13] by employing different stabilizers,[1] and by light irradiation and heat agitation,[14] respectively.

More recently, several 2D single-crystalline Ag nanoplates have been demonstrated by such a facile synthesis, mainly for the plasmonic/optoelectronic applications;[15] nevertheless, most of those synthesized single-crystalline Ag nanoplates are within a submicron scale,[16,17] still too small to replace the thin film fabricated by conventional physical depositions. Therefore, to accommodate more nanopatterned structures on a continuous plasmonic/optoelectronic platform,[18] herein we developed a HNO_3-assisted polyol reduction method to successfully fabricate ultralarge single-crystalline Ag microplates, whose lateral size is up to 50 μm, a maximum value so far based on the best of our knowledge. By introducing HNO_3, it activates the desorbed cyanide ions (CN^-) for ethylene glycol (EG) to reduce Ag on the (100) facets of the single-crystalline Ag plate to enhance its lateral size.[19] Furthermore, single-crystalline Ag microplates present the outstanding plasmonic property of the synthesized Ag microplates by demonstrating a far propagation length of surface plasmon polaritons (SPPs) of 11.22 μm at 534 nm excitation. The approach gives rise to the construction of a large-area 2D Ag plasmonic platform with high single crystallinity, buffer layer free, and versatile use on arbitrary substrates.

EXPERIMENTAL SECTION

Silver nitrate ($AgNO_3$), polyvinylpyrrolidone (PVP, M_w = 55 000 Da), nitric acid (HNO_3, 65 wt %), and ethylene glycol (EG) were purchased from Sigma-Aldrich and were not subjected to further purification. In the typical process, 1 mL HNO_3 was added to the 250 mg/75 mL of PVP/EG mixture with magnetic stirring. Subsequently, 150 mL of a 0.03 M aqueous $AgNO_3$ solution was added. The mixture was aged in a sealed glass bottle at 152 °C for 2, 4, 12, and 36 h. To control the concentrations of HNO_3 and EG, we only changed HNO_3 and EG to the total concentrations of 6.89×10^{-5}, 3.37×10^{-4}, and 4.67×10^{-4} M and 1.06×10^{-2}, 8.88×10^{-3}, 7.62×10^{-3}, and 5.93×10^{-3} M in an ambient

Received: April 27, 2014
Accepted: July 2, 2014
Published: July 2, 2014

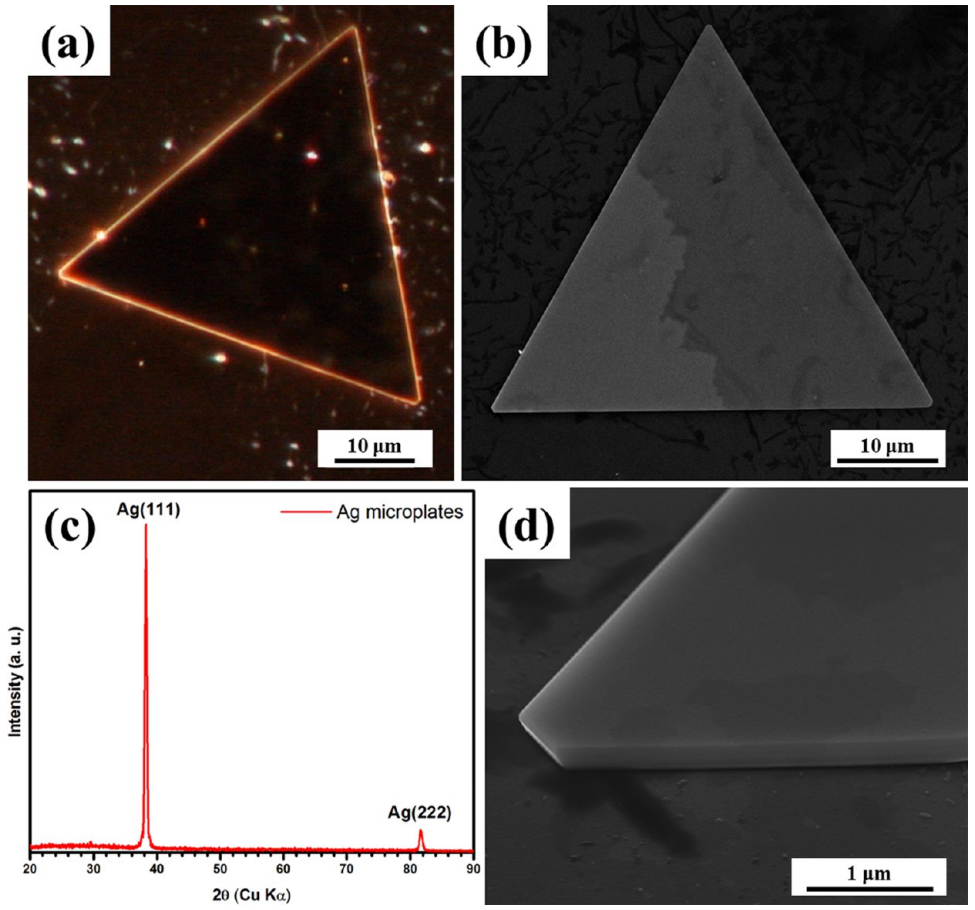

Figure 1. (a) Dark-field OM image and (b) SEM image of Ag microplate show that the lateral size is 47.5 μm. (c) XRD patterns of Ag microplates on glass substrate show the strong peak at Ag(111) and the reflectance at Ag(222), respectively. (d) 52° tilted SEM image of a magnified side view shows that the truncated edge possesses the flat top surface with a thickness of 290.3 nm.

atmosphere, respectively. (Caution: The dose of $HNO_{3\ (aq)}$ should be controlled carefully. An excessive dose can cause a severe explosion.) Note that the color changes rapidly from red, through muddy dark blue, to gray color as shown in Figure S1a–c in the Supporting Information. Finally, Ag microplates were washed with isopropanol and deionized water by using an ultrasonication and centrifugation sequence at least 4 times. Scanning electron microscopy (SEM; Jeol JSM-7000F), dual-beam focused ion beam (DB–FIB; FEI Nova-200 NanoLab Compatible), and X-ray diffraction (XRD; Shimadsu XRD 6000) were conducted to analyze the morphology and crystallinity of the as-synthesized Ag microplates. Linear sweep voltammetry (LSV) scanning measurement was conducted as described in previous studies,[20,21] and Ag microplates were replaced. High-resolution transmission electron microscopy (HRTEM; Jeol JEM-2100, Cs-corrected) was conducted to examine the single crystallinity at the atomic scale.

RESULTS AND DISCUSSION

In a typical polyol reduction process, an EG solvent serves as a reductant that reduces the Ag^+ to Ag^0,[22] thus forming trimeric nanoclusters.[23] Through the coalescence of Ag^0, the nucleated trimers grow to form Ag nanoplates with a twinned plane parallel to the (111) facets and PVP provides steric stabilization,[24] which involves the lateral growth of (100) facets in the presence of Ag^0 absorption and CN^- desorption.[19] However, using the rivalrous growth method limits the lateral size of the Ag nanoplates at the edge length of 3–5 μm.[19] We optimized the parameters to generate ultralarge Ag microplates, as shown in Figure 1. The dark-field optical microscopy image in Figure 1a shows a synthesized triangular Ag microplate with an edge length of nearly 46.8 μm; at this size, the microplate is visible to the naked eye. The triangular edge length was 47.5 μm, as shown in Figure 1b. The crystal orientation of the entire substrate was observed, and the XRD patterns in Figure 1c show high orientation at (111) facets and reflection at (222).[25] The tilted SEM image shown in Figure 1d illustrates that the thickness of the microplate was 290.3 nm and that the top surface was flat. These depictions show that the lateral size of Ag microplates can be increased by optimizing the reaction time (12 h), temperature (152 °C), and reagent dose (EG = 5.93 mM and HNO_3 = 4.67 × 10^{-4} M) compared with other chemical routes.[16,17]

Figure 2 shows an HRTEM image of the edges and corners of a triangular Ag microplate. We selected the Ag microplate shown in the center; this microplate exhibited an edge length of 30 μm. The trio of corners and edges shown in Figure 2a–f reveals that a *d*-spacing of 0.14 nm corresponded with {220} and the top and bottom facets were (111). The face-centered cubic (fcc) forbidden $d_{1/3(422)}$ = 2.50 nm reflection[26,27] is not observable in the HRTEM images but is observable in the diffraction patterns (DPs) shown in Figure S2 (in the Supporting Information). It is reasonable to conclude that using the HNO_3-assisted polyol method enlarges the lateral size of Ag microplates to nearly 50 μm and enables high single crystallinity to be maintained with the anisotropic growth of top and bottom (111) facets.

To evaluate the evolution on the lateral size of Ag microplates, reaction periods of 2, 4, 12, and 36 h were used. A histogram of each period in Figure S3 in the Supporting Information was plotted by statistically calculating at least 500 pieces, and

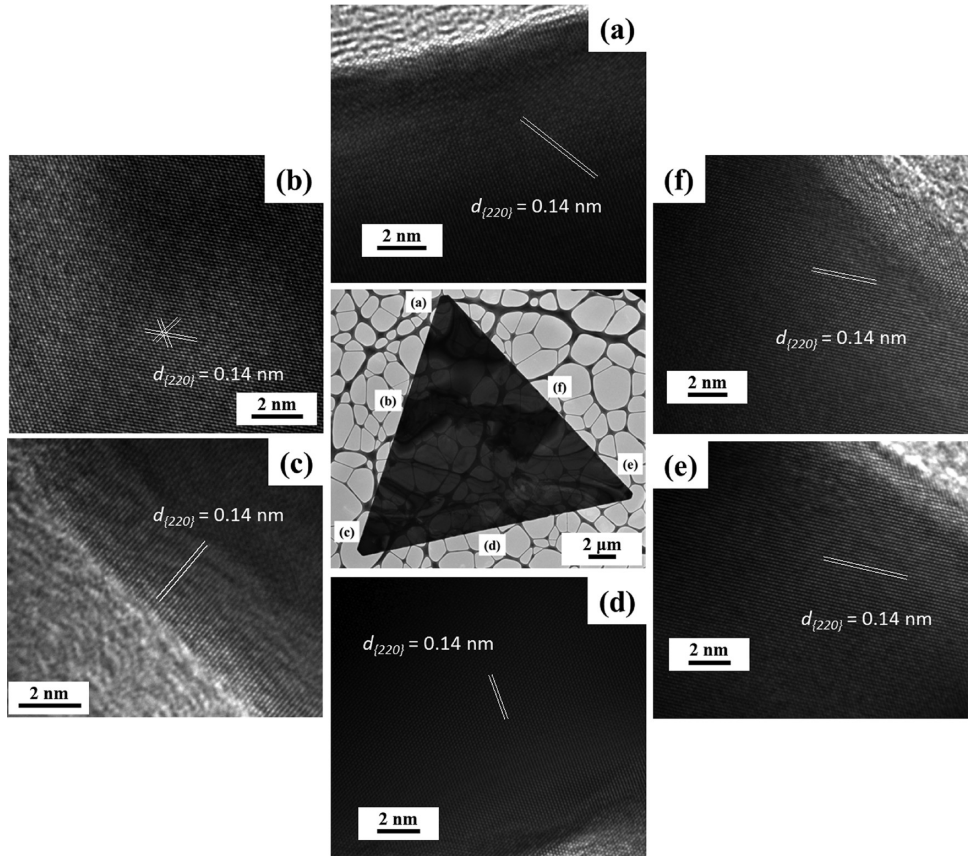

Figure 2. (a–e) HRTEM images of the single-crystalline Ag microplate show the $d_{(220)}$ = 0.14 nm at the trio of corners and edges with the top (111) facets.

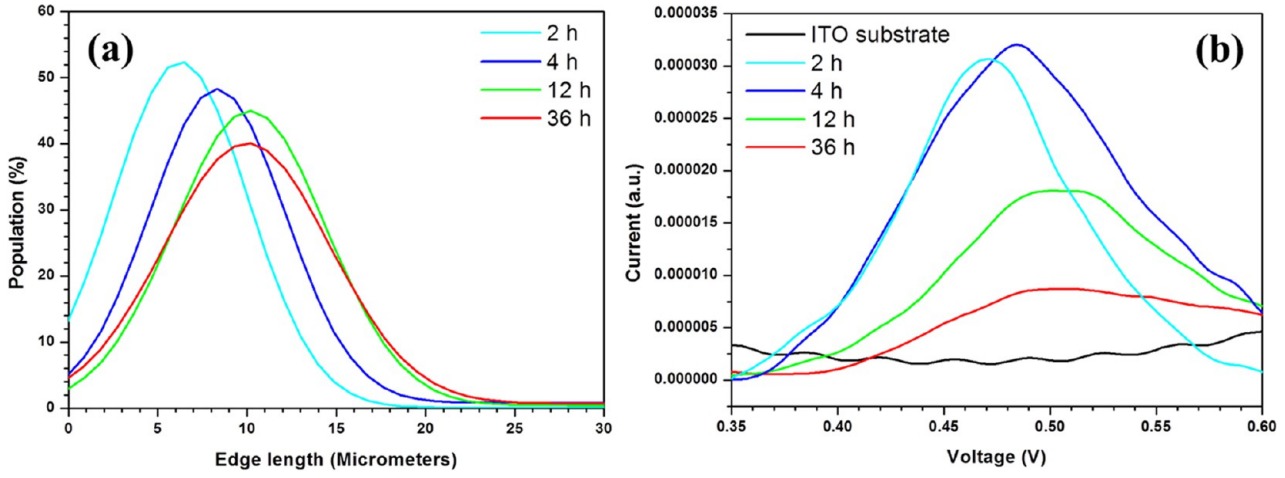

Figure 3. (a) Stacked Gaussian fitting curves from the histograms of Ag microplates (also see Figure S3 in the Supporting Information) and (b) linear sweep voltammetry (LSV) scanning measurement (Ag/AgCl and Pt act as the reference and counterelectrode in 0.1 M $H_2SO_{4\ (aq)}$ electrolyze) in the various reaction periods.

histograms were fitted according to a Gaussian distribution (*t*-test *p* values < 0.05). Note that the thickness of Ag microplates in different reaction periods was also calculated (Figure S4 in the Supporting Information). Figure 3a shows overlapped Gaussian fitting curves of the lateral size versus the periods of reaction time, indicating shifts for 6.53, 8.36, and 10.22 μm at 2, 4, and 12 h, respectively. The average edge lengths increased as the reaction time increased and reached a maximum of 10.22 μm at 36 h. Figure 3b shows the results of the LSV scanning measurement, revealing that the voltages exhibited a trend of increased shifting for 0.47, 0.48, 0.50, and 0.50 V at 2, 4, 12, and 36 h, respectively. Since the chemical potential energy decreases when the electrochemical oxidation potential increases with the surface-to-volume ratio,[21] the reaction becomes relatively stable, and the maximal lateral size is reached during periods of 12–36 h.

According to the foregoing discussion, the growth of a single-crystalline Ag microplate strongly depends on solvent reduction and surfactant stabilization.[28] Therefore, EG plays a crucial role in the nucleation and growth of large Ag microplates. Parts a–d of Figure 4show SEM images of EG in various concentrations.

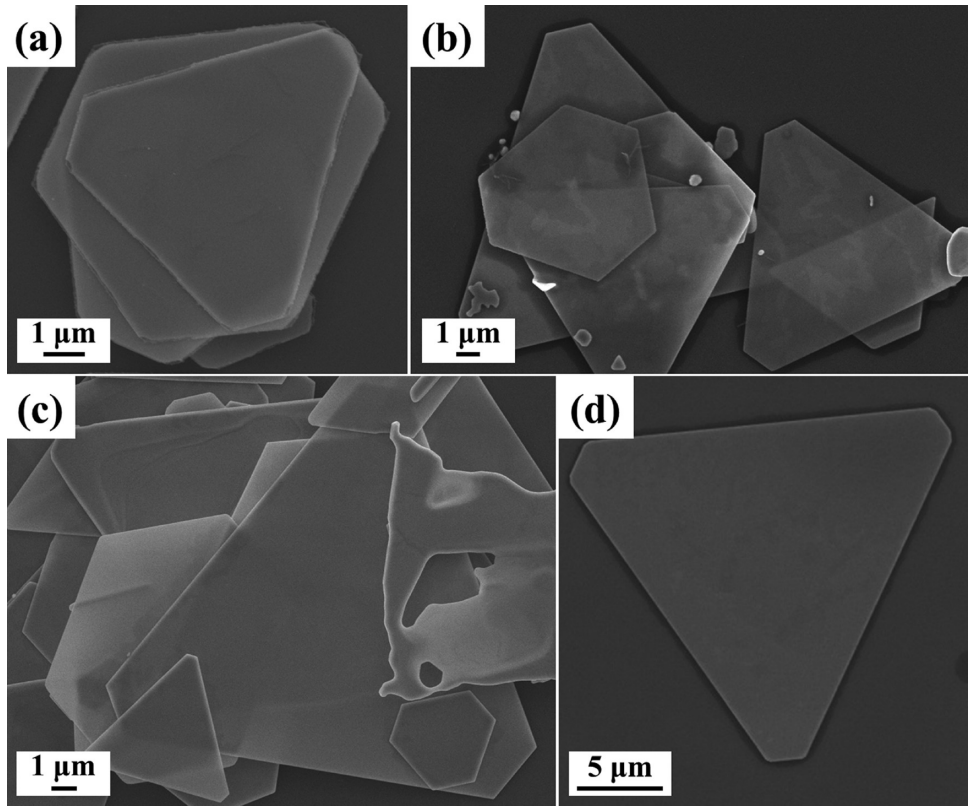

Figure 4. Various concentrations of solvent EG, (a) 1.06×10^{-2}, (b) 8.88×10^{-3}, (c) 7.62×10^{-3}, and (d) 5.93×10^{-3} M, show that the lateral sizes of Ag microplates are corresponding to 6, 13, 15, and 23 μm, respectively.

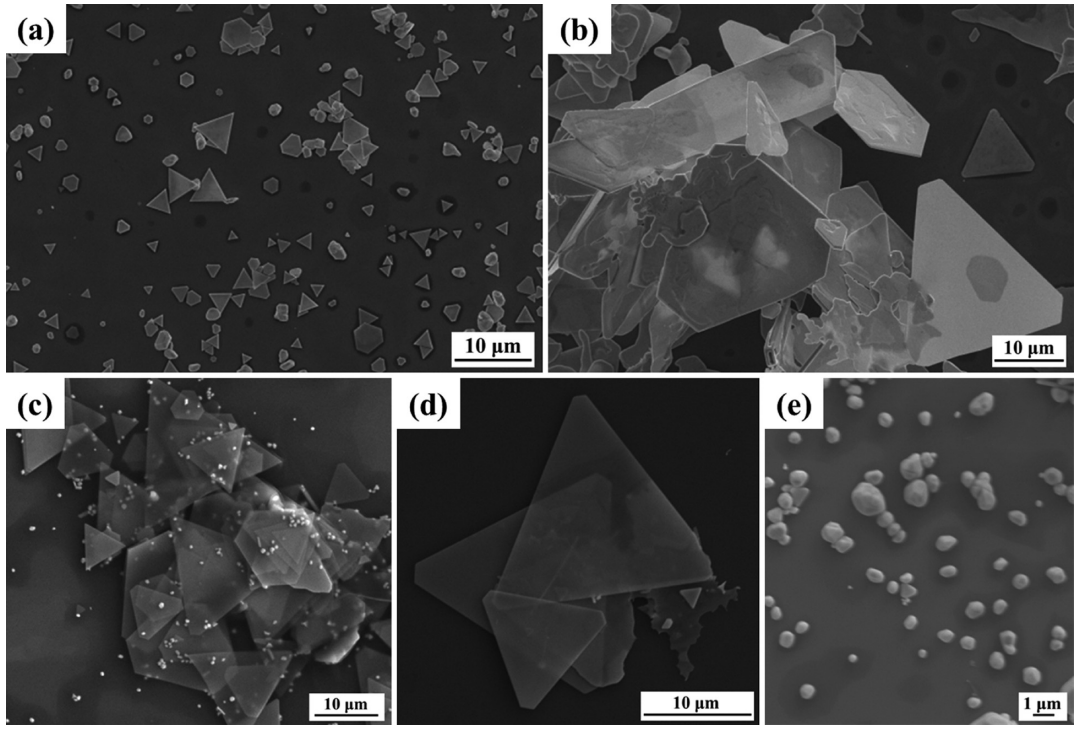

Figure 5. SEM images of Ag microplates with various concentrations of HNO_3, (a) without HNO_3, (b) 6.89×10^{-5}, (c) 3.37×10^{-4}, (d) 4.67×10^{-4} M, and (e) without polyvinylpyrrolidone (PVP) polymer, show that the lateral size of Ag microplates increased with the relative high concentrations of HNO_3 and stops increasing at the concentration of 4.67×10^{-4} M.

Note that the lateral size distribution and thickness in various concentrations of EG are shown in Figures S5 and S6 in the Supporting Information. At a high concentration of 1.06×10^{-2} M, numerous Ag^0 are reduced by EG; hence, nucleation is faster than the growth, so supersaturated precipitates in the mixture form a small Ag microplate at a lateral size of up to 6 μm. The

Scheme 1. Growth Mechanism of Ultralarge Ag Microplates by Using HNO_3-Assisted Polyol Method[a]

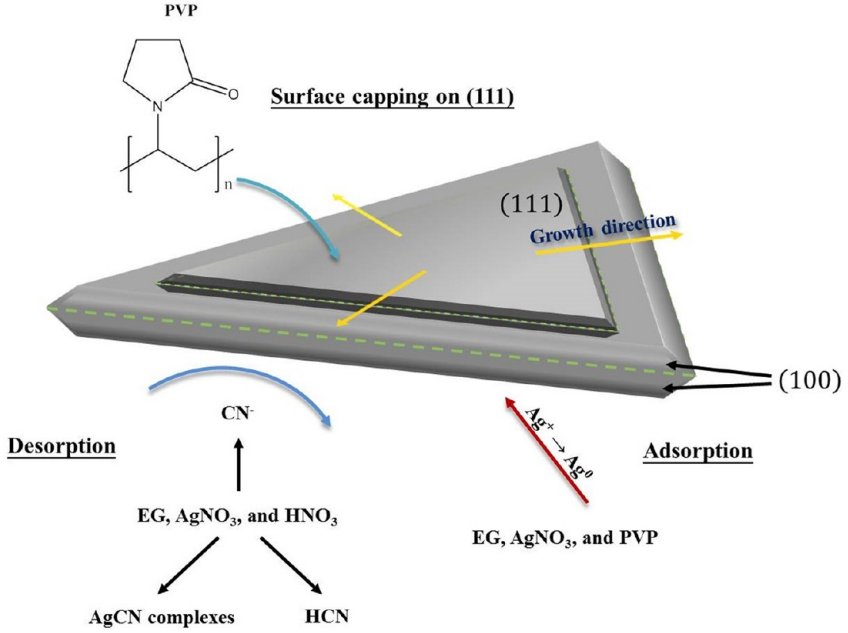

[a]Polyvinylpyrrolidone (PVP) polymer acts as a steric stabilizer on the top and bottom (111) facets, and the cyanide ions (CN^-) desorb the occupied Ag^0 at the (100) facets. CN^- desorption forms the open vacancies and induces the absorption of newly formed Ag^0 on the sites; it is noted that CN^- are formed by the ethylene glycol (EG), $AgNO_3$, and HNO_3.

results obtained in the initial stage of edge length distribution (Figure 3a) after 2 h of reaction time indicated that the high percentage of the small lateral size of Ag microplates can be attributed to similar supersaturated precipitates. As the concentration decreased, the growth process gradually dominated the reaction at the lateral size of 13, 15, and 23 μm, as shown in parts b, c, and d of Figure 4, respectively.

On the other hand, to make sure of the importance of desorption, we used another factor of HNO_3 when the concentration of EG was fixed at 5.93×10^{-3} M and the reaction time was fixed at 12 h. Figure 5a shows a mixture without HNO_3, which yielded Ag microplates with a lateral size of only 6−8 μm. However, the lateral size substantially increased to 24 μm when 6.89×10^{-5} M HNO_3 was used, as shown in Figure 5b, indicating that HNO_3 increases the lateral size of Ag microplates. Note that the lateral size distribution in various concentrations of HNO_3 is shown in Figure S7 in the Supporting Information. When the concentration of HNO_3 was increased to 3.37×10^{-4} and 4.67×10^{-4} M, the lateral size did not change substantially; however, the top facets became flat and smooth, as shown in Figures 5c and d and S8 in the Supporting Information. Figure 5e shows that PVP was absent and only nanoparticles were observed because PVP can serve as a steric stabilizer[24] and reduces Ag^+ to Ag^0,[22] indicating the importance of the surfactant in forming Ag microplates.

To clarify the lateral size increase of ultralarge Ag microplates fabricated using the HNO_3-assisted polyol method, we suggest a possible growth mechanism, as shown in Scheme 1. Nucleated fcc triangular Ag plate-like nanoseeds are bounded with three (100) side facets and two (111) top facets[29,30] where the twinned plane is parallel to the (111) facets so that the lateral size can be increased by extending the [100] directions.[28] EG plays a role in the reduction of Ag^0 according to the following reaction equations:

$$2HOCH_2CH_2OH \rightarrow 2CH_3CHO + 2H_2O \quad (1)$$

$$2AgNO_3 + 2CH_3CHO \rightarrow CH_3COCOCH_3 + 2Ag + 2HNO_3 \quad (2)$$

$$4HNO_3 + 3Ag \rightarrow 3AgNO_3 + NO + 2H_2O \quad (3)$$

Equations 1 and 2 represent the formation of EG-reduced Ag^0,[31] providing the nucleation and growth processes. The reaction rate can be controlled by tuning the EG concentrations. The reaction among $AgNO_3$, HNO_3, and EG produces an etching (CN^-),[32] which is prone to react with Ag^+ and H^+ from the dissolved $AgNO_{3(aq)}$ and $HNO_{3(aq)}$. Parts a−c of Figure S9 in the Supporting Information show an SEM image with an energy-dispersive spectroscopy (EDS) spectrum indicating that spike-like AgCN wires were present, which was confirmed according to the corresponding XRD pattern. Luo et al. reported that PVP does not need to be considered in the reaction because precipitated AgCN wires still existed in the absence of PVP during the reaction.[19] Because of the strong binding force of $C\equiv N^- > C{=}O$ and the surface energy of Ag (100) > (111),[28] a CN^- serves as the etching reagent. Desorption occurs on (100)-dominated rather than on (111), which is stabilized by PVP. Furthermore, as illustrated in eq 3, $HNO_{3(aq)}$ induces CN^- formation, thus opening additional vacant sites for Ag^0 adsorption, and directly etches Ag, thus tailoring the newly formed edge of Ag microplates.[19] The top and bottom facets become flat and smooth when concentrations of $HNO_{3(aq)}$ are increased, as shown in Figure 5b−d. Therefore, the key factors for increasing the lateral growth of Ag microplates are the concentrations of EG and $HNO_{3(aq)}$, which influence the reduction of Ag^0 absorption and the formation of CN^- desorption.

The remarkably large area and reliable thickness of the fabricated single-crystalline Ag microplates is suitable for

optoelectronic applications.[1−6] The applications strongly depend on SPPs because the electron oscillations are plasmonically collected, the electromagnetic waves are concentrated, and the electric fields propagate on the metal−dielectric interface.[33] However, regarding propagation length, loss from material surface roughness and grain boundaries[34] dominates the quality of optoelectronic devices (Figure S10 in the Supporting Information). To determine the value of propagation length, we employed FIB patterning on the Ag microplate and assumed that SPPs traveled from the input to output silts on various paths, as shown in Figure 6a. Figure 6b shows an SEM image of a geometric configuration with a maximal distance of 20 μm. A focused 534 nm laser with 90° polarized incidence, perpendicular to the input silt, excited in-coupling SPP propagation at the air/Ag interface through the output of transmitted radiation, as shown in Figure 6c. The dielectric function of metallic Ag (ε_m) can be expressed as

$$\varepsilon_m = \varepsilon_m' + i\varepsilon_m'' \tag{4}$$

According to the Drude model, the wave vector (k_x) propagating along the direction of the air/Ag interface can be expressed as[34,35]

$$k_x = k_x' + ik_x'' = \frac{\omega}{c}\sqrt{\frac{\varepsilon_m'}{\varepsilon_m' + 1}} + i\frac{\omega}{c}\left(\frac{\varepsilon_m'}{\varepsilon_m' + 1}\right)^{3/2}\frac{\varepsilon_m''}{2\varepsilon_m'^2} \tag{5}$$

, where the wave vector can be expressed in terms of its real and imaginary parts (k_x' and k_x''). The terms ω and c represent the angular momentum and light speed, respectively; thus, the SPP propagation length (L_{SPPs}) is given by

$$L_{SPPs} = \frac{1}{2k_x''} \tag{6}$$

The intensity at the output silts can be quantitatively measured using a charge-coupled device (CCD) camera (MD-130 digital microscope camera). The following fitting equation is used after calculating the SPP propagation length:[34−36]

$$\frac{\ln(I(d))}{\ln I_0} = 1 + \frac{-d}{L_{SPPs}\ln I_0} \tag{7}$$

, where $I(d)$ and I_0 are intensities at different distances (d) between the input and output and at the input position. Figure 6d shows a comparison of fitting curves for the single-crystalline Ag microplate and the E-gun-evaporated multicrystalline Ag thin film. The propagation lengths (L_{SPPs}) of the single crystal and multicrystal shows 11.22 and 5.27 μm, respectively, confirming that ultralarge single-crystalline Ag microplates are suitable for a 2D plasmonic platform.

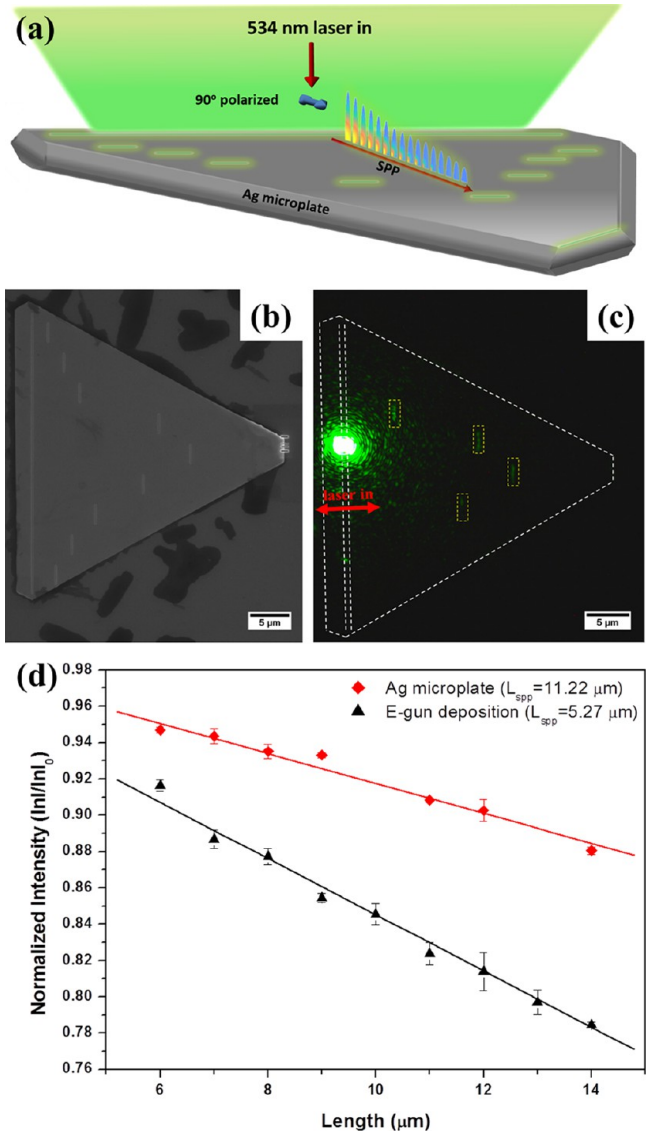

Figure 6. (a) Schematic for the Ag microplate with the input and output silts shows that a polarized 534 nm laser source (normal to the input slit) excites the surface plasmon polaritons (SPPs) propagation with an evanescent field on air/Ag interface. (b) SEM images of focused ion beam (FIB) milled silts with various distances between the input and output positions. (c) Optical image of polarized 534 nm laser source focused on the input position, coupling the transmitted radiation to the output silts. (d) Plots of normalized intensity versus the length of input−output silts, showing that the calculated SPPs propagation lengths of Ag microplate and E-gun-evaporated Ag thin film are 11.22 and 5.27 μm, respectively.

CONCLUSIONS

In this paper, we report the facile synthesis of ultralarge single-crystalline Ag microplates fabricated using the HNO_3-assisted polyol reduction method. First, a high-resolution TEM analysis revealed that the fcc lattice structure of the fabricated Ag microplates consisted of $d_{\{220\}}$ = 0.14 nm and the forbidden $d_{1/3(422)}$ = 2.50 nm, corresponding to the top (111) facets and the twinned plane parallel to the (111). The high-quality crystallinity of the Ag microplates, which featured an edge size reaching 50 μm, is the maximal value obtained according to our extensive review of relevant research. Furthermore, the size distribution with respect to various reaction times ranging from 2 to 36 h showed that the optimal trend occurred at 12 h, which is consistent with the results of LSV scanning measurements. These measurements indicated that the electrochemical oxidation potential exhibited a relatively stable state at the reaction time of 12 h. Second, when the HNO_3-assisted polyol reduction method is applied, solvent EG functions as a reduction agent of Ag^+, which grows on uncapped Ag (100) facets. In addition, HNO_3 plays a crucial role in dissolving Ag, providing open sites for Ag^0 adsorption to enhance growth on (100). Therefore, when the cyclic reaction among the solvent EG, $AgNO_3$, and HNO_3 is controlled carefully, the adsorption of Ag^0 and desorption of HNO_3 (CN^-) collectively react to increase the

lateral size and to maintain the flat top and bottom facets simultaneously. Finally, the ultralarge single-crystalline Ag microplates exhibited an excellent plasmonic property of reduced loss absorption. Under 534 nm laser excitation, the measured propagation length of SPPs was 11.22 μm, which is much greater than that of E-gun-evaporated Ag thin films (5.27 μm). We expect that further improving this HNO_3-assisted polyol reduction method will increase the lateral size of Ag microplates to submillimeter scale, providing an outstanding plasmonic platform that benefits integrated optoelectronic applications.

■ ASSOCIATED CONTENT

Supporting Information

Supplementary figures of the results including experimental setup, TEM diffraction patterns at the trio of corners and edges, lateral size and thickness of Ag microplates in various reaction periods, lateral size and thickness distribution in various concentrations of EG and concentrations of HNO_3, characterizations of AgCN wires, and a comparison between single crystals and multicrystals focused ion beam (FIB) patterning. This material is available free of charge via the Internet at http://pubs.acs.org.

■ AUTHOR INFORMATION

Corresponding Author

*Tel.: 886-3-5742171. Fax: 886-3-5722366. E-mail: tjyen@mx.nthu.edu.tw.

Notes

The authors declare no competing financial interest.

■ ACKNOWLEDGMENTS

The authors would like to gratefully acknowledge the financial support from the Ministry of Science and Technology (101-2628-E-007-016-MY3, 102-2221-E-007-113-MY4, and 102-2811-P-007-002) and the Ministry of Education ("Aim for the Top University Plan" for National Tsing Hua University under project numbers 102N2015E1 and 102N2043E1).

■ ABBREVIATIONS

$AgNO_3$, silver nitrate
CN^-, cyanide ions
DB−FIB, dual-beam focused ion beam
EDS, energy-dispersive spectroscopy
EG, ethylene glycol
HNO_3, nitric acid
HRTEM, high-resolution transmission electron microscopy
LSV, linear sweep voltammetry
PVP, polyvinylpyrrolidone
SEM, scanning electron microscopy
SERS, surface-enhanced Raman scattering
SPPs, surface plasmon polaritons
XRD, X-ray diffraction

■ REFERENCES

(1) Zeng, J.; Xia, X.; Rycenga, M.; Henneghan, P.; Li, Q.; Xia, Y. Successive Deposition of Silver on Silver Nanoplates: Lateral versus Vertical Growth. *Angew. Chem., Int. Ed.* **2011**, *50*, 244−249.

(2) Homan, K. A.; Souza, M.; Truby, R.; Luke, G. P.; Green, C.; Vreeland, E.; Emelianov, S. Silver Nanoplate Contrast Agents for in Vivo Molecular Photoacoustic Imaging. *ACS Nano* **2012**, *6*, 641−650.

(3) Li, W.; Kuai, L.; Qin, Q.; Geng, B. Ag-Au Bimetallic Nanostructures: Co-reduction Synthesis and Their Component-Dependent Performance for Enzyme-free H_2O_2 Sensing. *J. Mater. Chem. A* **2013**, *1*, 7111−7117.

(4) Wu, Y. R.; Hollowell, A. E.; Zhang, C.; Guo, L. J. Angle-Insensitive Structural Colours based on Metallic Nanocavities and Coloured Pixels beyond the Diffraction Limit. *Sci. Rep.* **2013**, *3*, 1194−1199.

(5) Lin, D.; Huang, J. S. Slant-gap Plasmonic Nanoantennas for Optical Chirality Engineering and Circular Dichroism Enhancement. *Opt. Express* **2014**, *22*, 7434−7445.

(6) Wei, H.; Li, Z.; Tian, X.; Wang, Z.; Cong, F.; Liu, N.; Zhang, S.; Nordlander, P.; Halas, N.; Xu, H. Quantum Dot-Based Local Field Imaging Reveals Plasmon-Based Interferometric Logic in Silver Nanowire Networks. *Nano Lett.* **2011**, *11*, 471−475.

(7) Liu, H.; Wang, B.; Leong, E. S. P.; Yang, P.; Zong, Y.; Si, G.; Teng, J.; Maier, S. A. Enhanced Surface Plasmon Resonance on a Smooth Silver Film with a Seed Growth Layer. *ACS Nano* **2010**, *4*, 3139−3146.

(8) He, Y.; Shi, G. Surface Plasmon Resonances of Silver Triangle Nanoplates: Graphic Assignments of Resonance Modes and Linear Fittings of Resonance Peaks. *J. Phys. Chem. B* **2005**, *109*, 17503−17511.

(9) Chen, L.; Fu, X.; Lu, W.; Chen, L. Highly Sensitive and Selective Colorimetric Sensing of Hg^{2+} Based on the Morphology Transition of Silver Nanoprisms. *ACS Appl. Mater. Interfaces* **2013**, *5*, 284−290.

(10) Li, X.; Wang, L.; Yan, G. Review: Recent Research Progress on Preparation of Silver Nanowires by Soft Solution Method and Their Applications. *Cryst. Res. Technol.* **2011**, *46*, 427−438.

(11) Yi, Z.; Xu, X.; Wu, X.; Chen, C.; Li, X.; Luo, B.; Luo, J.; Jiang, X.; Wu, W.; Yi, Y.; Tang, Y. Silver Nanoplates: Controlled Preparation, Self-assembly, and Applications in Surface-Enhanced Raman Scattering. *Appl. Phys. A: Mater. Sci. Process.* **2013**, *110*, 335−342.

(12) Chang, S.; Chen, K.; Hua, Q.; Ma, Y.; Huang, W. Evidence for the Growth Mechanisms of Silver Nanocubes and Nanowires. *J. Phys. Chem. C* **2011**, *115*, 7979−7986.

(13) Korte, K. E.; Skrabalak, S. E.; Xia, Y. Rapid Synthesis of Silver Nanowires Through a CuCl- or $CuCl_2$-mediated Polyol Process. *J. Mater. Chem.* **2008**, *18*, 437−441.

(14) Tang, B.; Xu, S.; Hou, X.; Li, J.; Sun, L.; Xu, W.; Wang, X. Shape Evolution of Silver Nanoplates through Heating and Photoinduction. *ACS Appl. Mater. Interfaces* **2013**, *5*, 646−653.

(15) Huang, J.; Callegari, V.; Geisler, P.; Bruning, C.; Kern, J.; Prangsma, J. C.; Qu, X.; Feichtner, T.; Ziegler, J.; Weinmann, P.; Kamp, M.; Forchel, A.; Biagioni, P.; Sennhauser, U.; Hecht, B. Atomically Flat Single-Crystalline Gold Nanostructures for Plasmonic Nanocircuitry. *Nat. Commun.* **2010**, *1*, 150−157.

(16) Du, J.; Han, B.; Liu, Z.; Liu, Y. Control Synthesis of Silver Nanosheets, Chainlike Sheets, and Microwires via a Simple Solvent-Thermal Method. *Cryst. Growth Des.* **2007**, *7*, 900−904.

(17) Chen, H.; Simon, F.; Eychmüller, A. Large-Scale Synthesis of Micrometer-Sized Silver Nanosheets. *J. Phys. Chem. C* **2010**, *114*, 4495−4501.

(18) Lee, H.; Jeong, K.; Kang, T.; Seo, M.; Kim, B. A Twin-free Single-crystal Ag Nanoplate Plasmonic Platform: Hybridization of the Optical Nanoantenna and Surface Plasmon Active Surface. *Nanoscale* **2014**, *6*, 514−520.

(19) Luo, X.; Li, Z.; Yuan, C.; Chen, Y. Polyol Synthesis of Silver Nanoplates: The Crystal Growth Mechanism Based on a Rivalrous Adsorption. *Mater. Chem. Phys.* **2011**, *128*, 77−82.

(20) Ivanova, O. S.; Zamborini, F. P. Size-Dependent Electrochemical Oxidation of Silver Nanoparticles. *J. Am. Chem. Soc.* **2010**, *132*, 70−72.

(21) Kuo, C. L.; Hwang, K. C. Does Morphology of a Metal Nanoparticle Play a Role in Ostwald Ripening Processes? *Chem. Mater.* **2013**, *25*, 365−371.

(22) Im, S. H.; Lee, Y. T.; Wiley, B.; Xia, Y. Large-Scale Synthesis of Silver Nanocubes: The Role of HCl in Promoting Cube Perfection and Monodispersity. *Angew. Chem., Int. Ed.* **2005**, *44*, 2154−2157.

(23) Xiong, Y.; Washio, I.; Chen, J.; Sadilek, M.; Xia, Y. Trimeric Clusters of Silver in Aqueous $AgNO_3$ Solutions and Their Role as Nuclei in Forming Triangular Nanoplates of Silver. *Angew. Chem., Int. Ed.* **2007**, *46*, 4917−4921.

(24) Murshid, N.; Kitaev, V. Role of Poly(vinylpyrrolidone) (PVP) and Other Sterically Protecting Polymers in Selective Stabilization of

{111} and {100} Facets in Pentagonally Twinned Silver Nanoparticles. *Chem. Commun.* **2014**, *50*, 1247−1249.
(25) Cui, X.; Li, C. M.; Bao, H.; Zheng, X.; Zang, J.; Ooi, C. P.; Guo, J. Hyaluronan-Assisted Photoreduction Synthesis of Silver Nanostructures: From Nanoparticle to Nanoplate. *J. Phys. Chem. C* **2008**, *112*, 10730−10734.
(26) Liu, Z.; Zhou, H.; Lim, Y. S.; Song, J.; Piao, L.; Kim, S. Synthesis of Silver Nanoplates by Two-Dimensional Oriented Attachment. *Langmuir* **2012**, *28*, 9244−9249.
(27) Courty, A.; Henry, A.; Goubet, N.; Pileni, M. Large Triangular Single Crystals Formed by Mild Annealing of Self-Organized Silver Nanocrystals. *Nat. Mater.* **2007**, *6*, 900−907.
(28) Xia, Y.; Xiong, Y.; Lim, B.; Skrabalak, S. E. Shape-Controlled Synthesis of Metal Nanocrystals: Simple Chemistry Meets Complex Physics? *Angew. Chem., Int. Ed.* **2009**, *48*, 60−103.
(29) Xiong, Y.; McLellan, J. M.; Chen, J.; Yin, Y.; Li, Z.; Xia, Y. Kinetically Controlled Synthesis of Triangular and Hexagonal Nanoplates of Palladium and Their SPR/SERS Properties. *J. Am. Chem. Soc.* **2005**, *127*, 17118−17127.
(30) Xiong, Y.; Washio, I.; Chen, J.; Cai, H.; Ki, Z.; Xia, Y. Poly(vinyl pyrrolidone): A Dual Functional Reductant and Stabilizer for the Facile Synthesis of Noble Metal Nanoplates in Aqueous Solutions. *Langmuir* **2006**, *22*, 8563−8570.
(31) Xiong, Y.; Siekkinen, A. R.; Wang, J.; Yin, Y.; Kim, M. J.; Xia, Y. Synthesis of Silver Nanoplates at High Yields by Slowing Down the Polyol Reduction of Silver Nitrate with Polyacrylamide. *J. Mater. Chem.* **2007**, *17*, 2600−2602.
(32) Collins, P. H.; Holloway, K. J. A Reappraisal of Silver Fulminate as a Detonant. *Propellants Explos.* **1978**, *3*, 159−162.
(33) Park, J. H.; Ambwani, P.; Manno, M.; Lindquist, N. C.; Nagpal, P.; Oh, S.; Leighton, C.; Norris, D. J. Single-Crystalline Silver Films for Plasmonics. *Adv. Mater.* **2012**, *24*, 3988−3992.
(34) Wild, B.; Cao, L.; Sun, Y.; Khanal, B. P.; Zubarev, E. R.; Gray, S. K.; Scherer, N. F.; Pelton, M. Propagation Lengths and Group Velocities of Plasmons in Chemically Synthesized Gold and Silver Nanowires. *ACS Nano* **2012**, *6*, 472−482.
(35) Raether, H. *Surface Plasmons*; Springer-Verlag: Berlin, 1988.
(36) Ma, Y.; Li, X.; Yu, H.; Tong, L.; Gu, Y.; Gong, Q. Direct Measurement of Propagation Losses in Silver Nanowires. *Opt. Lett.* **2010**, *35*, 1160−1162.